Accepted Manuscript online: 2021-03-22 Article published online: 2021-05-17

Organic Materials S. Naumann THIEME OPEN ACCESS Short Review

Strategies for Pore-Diameter Control in Mesoporous Carbons Derived from Organic Self-Assembly Processes

Stefan Naumann[*a]

[a] University of Stuttgart, Institute of Polymer Chemistry, Pfaffenwaldring 55, 70569 Stuttgart, Germany
stefan.naumann@ipoc.uni-stuttgart.de

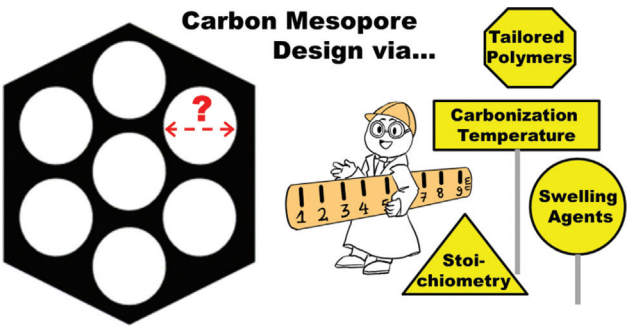

Received: 29.01.2021
Accepted after revision: 26.02.2021
DOI: 10.1055/a-1458-5109; Art ID: om-21-0017sr

Abstract Soft-templating techniques have greatly facilitated access to (ordered) mesoporous carbon materials. A key strength of these approaches is that the resulting material can be shaped by a multitude of parameters – rendering soft-templating inherently versatile regarding features such as pore arrangement or pore sizes. Nonetheless, rational manipulation of pore sizes/diameters, let alone a systematic variation thereof, remains a formidable challenge with high relevance for research fields as diverse as catalysis, sensing or energy storage and conversion. Thus, this Short Review aims to provide a structured account of the most frequently employed strategies to impact mesopore diameters in carbon materials derived via soft-templating.

Key words mesoporous carbons, soft-templating, pore size control

1. Introduction

(Ordered) mesoporous carbon materials (OMCs) have developed to be an attractive topic of inter-disciplinary research and are nowadays considered crucial for a number of key technologies.[1] This is down to a favorable combination of tunable properties, including a high surface area, significant pore volume, various pore sizes (i.e., micro-, meso- or macropores, including hierarchical setups), different types of ordered pore arrangements and connectivities (isolated pores vs. networks), electric conductivity, low density/weight and the possibility to readily modify surface functionalities or dope the bulk of the material with heteroelements (B, N, P).[2–5] Thus, depending on the desired application, very distinct property profiles can be realized, which is further emphasized by the fact that OMCs can be synthesized as powders, films,[6] monoliths[7] or as discrete particles.[8]

Accordingly, OMCs, and also disordered congeners, have found broad employment,[9–15] including application as electrode materials, for the immobilization of catalysts or the purification of drinking water. Many more examples could be named.

The advent of soft-templating approaches, complementing established hard-templating strategies, has been a major contributor to this positive trend.[16–18] Facilitating accessibility, scalability and broadening the scope of available target structures, soft-templating is currently used in many variations, but the basic principle remains the same. Typical components include (1) a carbon precursor, (2) a structure-directing agent (SDA) and (3) a solvent, if necessary. In some cases further additives, such as dopants or catalyst for the polymerization/cross-linking of the carbon precursor, are also added. Such a setup makes use of self-assembly phenomena, driven by the amphiphilic character of the SDA. The latter is typically a block copolymer with lipophilic and hydrophilic blocks. In an environment of suitable polarity, the actual nanostructured, three-dimensional organization often proceeds via the formation of micelles or micellar systems, whereby the hydrophilic corona strongly interacts with polar carbon precursors, which accordingly assemble around the micelles. Thus, SDA and carbon precursor must fit to the polarity profile of each other; further, the precursor should be of low molar mass, so as not to encumber the self-organization, and be polymerizable/cross-linkable in order to fix the three-dimensional mesostructure. Since template

Biosketches

Stefan Naumann: After finishing his PhD in 2014 in the group of Prof. M. R. Buchmeiser, Stefan Naumann was granted a DFG research stipend and he joined Prof. Andrew P. Dove at the University of Warwick (UK). Returning to University of Stuttgart (Germany) in 2015, he currently works on his habilitation in polymer chemistry. Since 2018 he is PI in the Collaborative Research Council (CRC) 1333 ("Molecular Heterogeneous Catalysis in Confined Geometries"). In 2019, he was awarded with an advancement stipend by the Macromolecular Division of the German Chemical Society (GDCh). His current research interests encompass the development of polymerization catalysts (organocatalysis, dual catalysis, organometallic single-site complexes) as well as the preparation of ordered mesoporous carbon materials and their application in catalysis.

removal is usually achieved by heating – the SDA component is burned off – an additional requirement for the (cross-linked) carbon precursor is a suitably high thermal stability. Finally, at higher temperature (>600 °C), the actual carbonization takes place, hence the precursor must be able to be transformed into an sp^2-carbon-rich matrix (which however still contains significant amounts of heteroatoms and is not comparable to graphite). Some of the more frequently employed polymeric SDAs and carbon precursors are depicted in Figure 1.

In a popular version of this approach, SDA and carbon precursor are mixed in a moderately polar and easily evaporating solvent (i.e., EtOH). The solution is then put into glass dishes, where the concentration of both components gradually rises as the solvent evaporates. At some point during this process (which can be surprisingly late) ordered structures are formed, and are later fixed by thermal curing (evaporation-induced self-assembly,[19] EISA).

While a detailed description of soft-templating processes for carbon material formation is available from excellent review literature,[20–23] a well-established and representative example shall be briefly discussed to illustrate the above considerations (Scheme 1). This approach, which was pioneered by Dai[24] and Zhao,[25] employs simple phenolic resin chemistry for both the generation of the carbon precursor and the stabilization of the formed mesostructure by cross-linking. In a first step, phenol (or resorcinol, phloroglucinol) is oligomerized with formaldehyde under basic conditions; this low molar mass compound ("resol", green) is the actual carbon precursor. Subsequently, the resol is mixed with the SDA, typically a triblock copolymer of the "*Pluronic*" family (PEO-*b*-PPO-*b*-PEO), in a specific ratio in ethanol. This mixture is then film-cast, using silicon wafers or simple glass surfaces, hence following the EISA process outlined above. Crucially, the carbon precursor molecules are polar compounds on account of the hydroxyl functionalities present. It should be noted that the concentration of the latter will heavily depend on the applied resin type (compare Figure 1). The –OH moieties ensure that a strong interaction with the polar corona of the formed micellar systems occurs (PEO blocks), yet at the same time inhibit migration of the resol into the nonpolar micellar cores (PPO) – a key requirement for the formation of ordered, porous assemblies.

The resulting colorless films are then subjected to a mild thermal treatment, for example 100 °C/24 h. During this time, the resol is thermally cured (fully cross-linked) and, ideally, the ordered mesostructure fixed. However, it should be noted

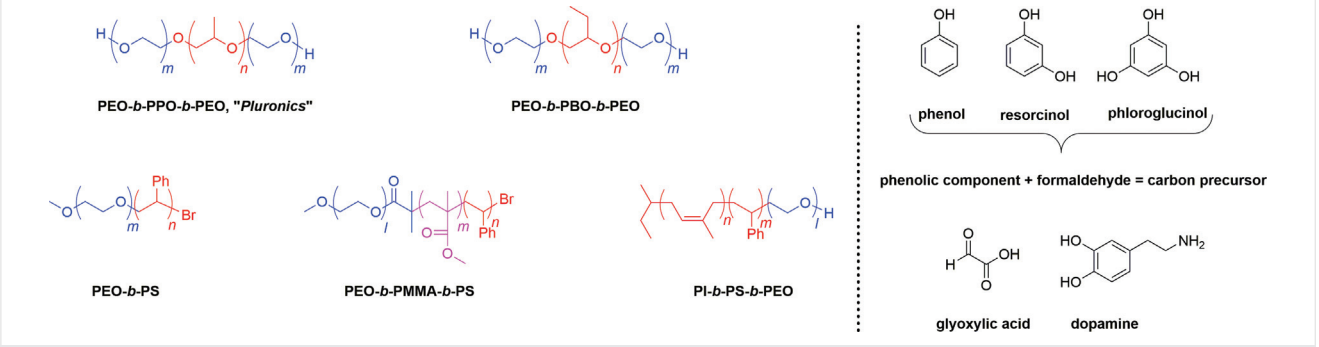

Figure 1 Compounds as discussed in this review. Left: Amphiphilic, structure-directing polymers (blue = hydrophilic, red = lipophilic moieties). Right: Carbon precursor components.

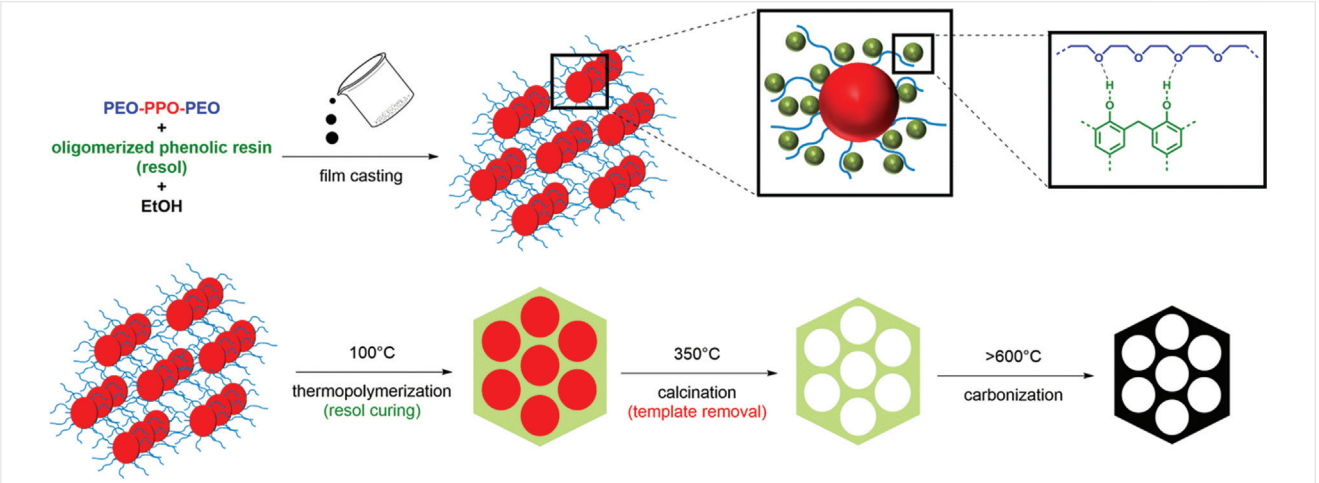

Scheme 1 OMC preparation via soft-templating, according to Zhao and Dai.[24,25]

that the thermal treatment itself can play a role in the actual structure formation, as has been underlined by Bein and co-workers.[26] The curing procedure is followed by further thermal treatment to achieve calcination and carbonization, frequently in a single work step using specifically tailored heating programs. Thereby, the cross-linked material can be processed in the form of flakes and powders, but also as a continuous film.[6] Typically, calcination (removal of the oxygen-rich, non-cross-linked template/SDA) occurs in the range of 300–400 °C.[3] In this example (Scheme 1), specifically the assembled micellar cores (PPO blocks, red) are burned off under protective gas, entailing the formation of a porous, polymeric structure, while the weight loss of the cross-linked matrix itself is much smaller.[2] A further increase in temperature then entails carbonization and ultimately delivers the final product.

Overall, this example nicely underlines the characteristic user-friendliness of soft-templating strategies, with the whole process being based on rapid and cheap chemistry and simple thermal treatment. This is in stark contrast to what is usually necessary for hard-templating syntheses (preparation of suitable mesoporous silica template, HF-etching); quite often, also more uniform and less fragile carbon mesostructures are received.

However, if a representative synthetic scheme such as depicted (Scheme 1) is considered in more detail, the sheer amount of parameters, which can impact structure formation, should be appreciated. This is especially relevant for a delicate property such as pore diameter. For example, if we consider a specific polymeric SDA, factors such as purity, molar mass distribution or end-group fidelity will be important, irrespective of whether commercial or lab-tailored polymers are employed. It is well known that polydispersity ($Đ_M$) impacts self-assembly.[27] Likewise, the presence and quantity of homopolymer impurities (i.e., PPO in *Pluronics*) can influence the micellar size (swelling phenomena) and change the overall hydrophilic to lipophilic balance (HLB). The same is even more pointedly true for the carbon precursor; if derived from step-growth oligomerization processes (as is the case for phenolic resins), one has to be aware of the limitations of this type of polymerization. Small changes in the pH, at which the resols are prepared, or the reaction time, or the temperature, will impact the characteristics of the oligomer mixture, most notably the average degree of polymerization. Quality control is therefore advisable (using gel-permeation chromatography or mass spectrometry), yet ideally the resol should be quickly used after preparation.

Accordingly, reproducible synthesis is dependent on precise protocolling and strict adherence to well-described procedures. Even slight changes will result in different materials, potentially also different pore dimensions, but this would not represent the degree of control and understanding which is necessary to realize optimized applications of OMCs, which are usually characterized by a pronounced dependency on specific pore dimensions.[28,29]

Hence, rational manipulation, let alone systematic variation, of the mesopore size (diameter, d_{Meso}) remains a challenging but crucial requirement to exploit porous carbon materials to the best extent. To provide some orientation, in the following several strategies to systematically impact this important feature are outlined, ranging from controlling the physical process conditions to precisely tuning the composition of polymeric SDAs.

2. Carbonization Temperature

Carbonization temperature is a powerful handle to influence numerous characteristics of the resulting material. It is also readily adapted in multi-step heating programs, simple to control and easily implemented without requiring much work effort. Choice of the protective atmosphere (N_2,

Ar) and the possibility to add reactive gases (such as oxygen) further extend applicability. Effective carbonization is usually achieved at $T > 600$ °C as a lower limit.[3] Very high carbonization temperatures can destroy the ordered structure by causing pore collapse or entail excessive formation of micropores, so that the majority of OMCs is prepared at the lower end of the carbonization temperature scale, frequently between 600 and 1400 °C. However, much harsher conditions have also been reported.[30]

Typical OMCs derived via the resol/*Pluronic* pathways display significant amounts of oxygen (i.e., even up to 17 wt% after carbonization at 800 °C)[3] and in general higher temperatures correspond to a lower degree of heteroatoms in the final product. Correspondingly, properties such as conductivity, density and also surface functionalities are heavily impacted.

This gradual change of composition, which goes alongside progressing compaction, entails shrinkage phenomena which can be exploited for the specific aim of pore-size control. While dependent on several factors – not least the question of whether powders (isotropic compaction) or films (uniaxial shrinkage) are carbonized – in general higher temperatures lead to smaller mesopores in the final carbon material. Thus, in an early example, Zhao compared samples with $Ia\bar{3}d$-symmetry (bicontinuous cubic), prepared via an aqueous route using a resol/*Pluronic* P123 (PEO_{20}-PPO_{70}-PEO_{20}) setup.[25] Investigating material obtained at 400 and 700 °C, nitrogen sorption showed that the mesopores shrank from 3.8 to 2.7 nm, while the wall thickness decreased from 4.2 to 3.6 nm, respectively. Simultaneously, the surface area expanded significantly (550 m^2/g vs. 1150 m^2/g). Such a behavior is quite typical for many OMCs and connected to the fact that the presence of micropores increases at higher carbonization temperature. Also, the usually relatively robust and thick-walled carbons retrieved from soft-templating become more fragile in the process, explaining why structural collapse can occur, in some case even at only 700 °C, as described by Song and co-workers.[31] In this contribution, a slightly different approach was employed [resorcinol (RF)-resin/*Pluronic* F108] to result in mesoporous carbon of the cubic $Im\bar{3}m$-type. Again the material obtained at 400 and 700 °C was directly compared, revealing a reduction of d_{Meso} from 6.3 to 4.9 nm. The broader pore size distribution of the OMC carbonized at $T = 700$ °C was attributed to partial pore collapse, in accordance with the fact that in this case the surface area only increased marginally.

Thermal stability of mesoporous carbons is strongly impacted by pore arrangement and synthetic details. Making use of this, Zhao and co-workers pushed OMC stability to 1400 °C and beyond, focusing this time on $p\bar{6}mm$-symmetry [two-dimensional (2D) hexagonal pore arrangement].[32] Based on resol/*Pluronic* F127, carbon materials were prepared under identical conditions with systematic variation of the applied carbonization temperature. The achieved d_{Meso} values spanned a range of 6.8 nm (350 °C) to 2.2 nm (1400 °C). A very similar tendency could be reproduced in the same work for cubic $Im\bar{3}m$-type material (Table 1). Importantly, while shrinkage is significant at lower temperature, from 600 °C on the effect is less pronounced. In a follow-up work, the same group could later show that further fine-tuning of the pore sizes is possible by feeding a small amount of oxygen (2.4 vol%) into the protective atmosphere of the carbonization oven.[33] Thus, it was found that at the same temperature of 350, 400, 800 and 1200 °C pore diameters of 5.4/7.1, 4.9/6.6, 4.3/3.1 and 2.8/3.1 nm were generated (Ar vs. N_2/O_2 atmosphere, 2D hexagonal OMC based on resol/F127). The presence of the small amount of O_2 facilitated template removal, allowing for the realization of larger mesopores without degrading the ordered structure of the carbon material, as evidenced by nitrogen sorption and well-resolved X-ray diffraction patterns. This approach also worked to similar effect for OMC with cubic $Im\bar{3}m$-symmetry.[33]

Table 1 Correlation of mesopore diameter and carbonization temperature according to Zhao[32]

Carbonization temperature [°C]	$p\bar{6}mm$-type d_{Meso} [nm][a]	$Im\bar{3}m$-type d_{Meso} [nm][a]
350	6.8	6.8
400	4.5	—
500	3.4	5.2
600	3.0	4.0
700	3.0	4.0
800	3.1	3.8
900	2.9	3.7
1200	2.7	3.1
1400	2.2	4.1

[a]Determined via nitrogen sorption.

Strikingly, OMCs can also be obtained at temperatures above 2000 °C. Targeting 2D hexagonal pore arrangement using a specific, acid-catalyzed preparation procedure based on resorcinol/formaldehyde and F127, Dai and co-workers prepared a carbon material which retained its mesostructures even when subjected to carbonization at 2600 °C.[30] Indeed, when comparing the nitrogen sorption results for materials heated to five different temperatures between 850 and 2600 °C (Figure 2), it was found that d_{Meso} was practically unchanged in a range of 6.3–6.6 nm. While at higher temperature the pore size distribution became somewhat broader and the surface area gradually shrank, the latter indicative of partial pore collapse or micropore removal, the mesostructure was overall surprisingly well retained. Wide-angle X-ray scattering analysis also underlined that in this case the material can indeed be rightfully described as graphitized OMC.

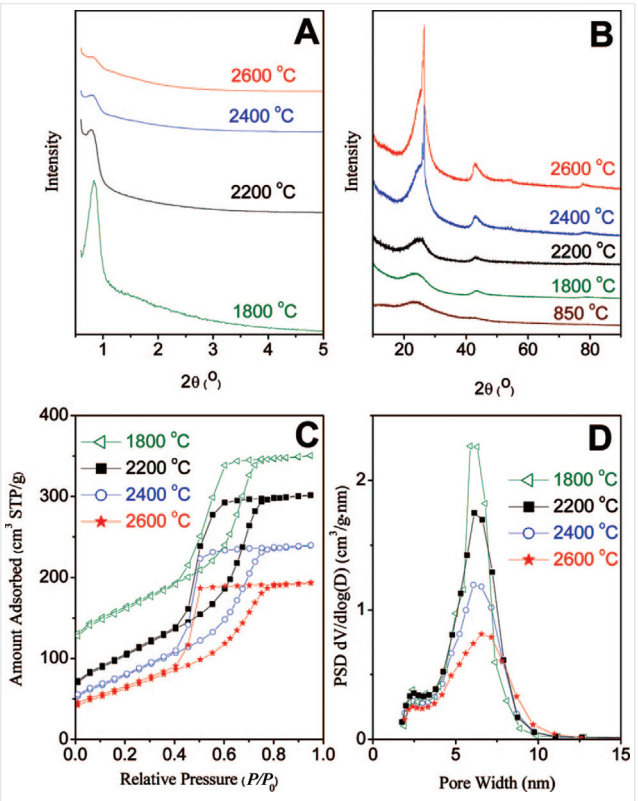

Figure 2 SAXS and WAXS analysis (A, B), N_2 isotherms (C) and pore size distribution (D) of OMC derived via an acidic synthesis route according to Dai. Reprinted with permission from Ref. 30. Copyright 2008 American Chemical Society.

The authors attributed the high thermal stability to the synthetic pathway. Acidic conditions entail a quick and thorough cross-linking of the resorcinol-based resin, rendering it rigid and potentially less susceptible to shrinking. This once again highlights that pore-diameter control via adaption of the carbonization temperature is not generally applicable but rather dependent on the employed chemical and catalytic setups.

As a general limitation regarding use of carbonization temperature to impact d_{Meso}, it should be considered that, strictly speaking, a systematic screening of pore-diameter impact on a specific application will be distorted by the fact that at higher carbonization temperature an impoverished surface chemistry will be obtained. Although rarely reported in studies targeting OMCs, the gradual loss of heteroatoms will result in a decreased density of, i.e., –OH/nm^2, alongside a loss of pore (wall) polarity. This, however, is a crucial property, regarding diffusion and adsorption, but also catalyst immobilization or electrochemical behavior.

3. Stoichiometry

Stoichiometric manipulation of the synthetic setup, such as the ratio of carbon precursor to SDA, is one of the most obvious approaches to exert a measure of control over the resulting pore sizes. Most frequently, this tuning parameter is employed with the specific aim to alter the type of pore arrangement. When considering the typical sequence of mesostructures that is obtained upon a stepwise increase of polarity (= growing HLB) in liquid crystal templating [lamellar, bicontinuous cubic ($Ia\bar{3}d$), hexagonal ($p\bar{6}mm$), body-centered cubic ($Im\bar{3}m$)], it is clear that this can be mimicked by tailoring the interaction of polar carbon precursor and amphiphilic block copolymer.[33]

Thus, for the resol/*Pluronic* system already mentioned above, a higher phenol-to-SDA ratio has similar repercussions as would result from an increase of the PEO mass fraction. This is because of the strong interaction of the phenolic hydroxyl functionalities with the polar ethylene oxide(EO)-derived repeat units – the hydrophilic volume effectively increases. The system has to accommodate the corresponding curvature at the PEO/PPO interface and assemble accordingly.

Using P123 (PEO_{20}-PPO_{70}-PEO_{20}) and increasing the ratio of phenolic components will hence transform the target mesostructure from lamellar over bicontinuous cubic to hexagonal, while F127 (PEO_{106}-PPO_{70}-PEO_{106}), a significantly more polar SDA, already starts out at the hexagonal pore arrangements and can even be pushed to the body-centered cubic order (Figure 3). This behavior already hints at the fact that SDA tailoring is an excellent venue for advanced pore-diameter control (see Section 5).

Nonetheless, stoichiometric variations can also be employed to effect more subtle changes, such as manipulation of the wall thickness or of d_{Meso}. Apart from the

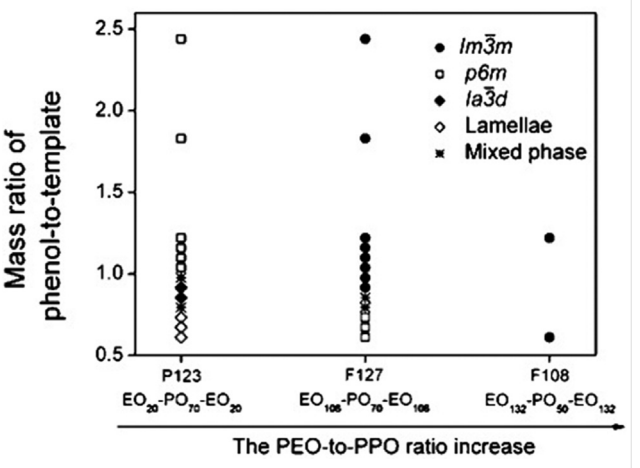

Figure 3 Phase diagram according to Zhao. Reprinted with permission from Ref. 33. Copyright 2006 American Chemical Society.

precursor/SDA ratio,[34,35] this can also involve variations of the solvent mixture[36] or variation of the content of cross-linking species (i.e., formaldehyde and derivatives).[37,38]

For example, in 2017, De Clercq and co-workers investigated a system based on resorcinol/formaldehyde (acid-catalyzed cross-linking) and F127.[34] They varied both the ratio of phenolic component to *Pluronic* SDA with mass ratios of 0.83, 0.5 and 0.25 as well as the carbonization temperature (400, 800, 1200 °C) and determined the textural properties of the received porous carbon material. While at a high ratio (0.83) well-defined, 2D hexagonal pore arrangement and narrow pore size distribution were achieved, a lower ratio of resorcinol entailed the generation of disordered structures and rather broad pore size distributions. Overall, a mesopore range of 7–50 nm was roughly addressable, whereby the impact of ratio variation on d_{Meso} was much more significant than the different carbonization temperatures. Thus, at a ratio of 0.85, pore diameters were in the range of 6–7 nm, while at 0.5 and 0.25 this increased to 21–30 and 40–44 nm, respectively.

Likewise, employing an acid-catalyzed ($HCl_{(aq)}$) resorcinol/formaldehyde-based setup, Nishiyama and co-workers could show that d_{Meso} of the resulting $p\bar{6}mm$-type OMC could be increased from 4.7 to 5.8 nm.[35] Again, the larger pore diameter was realized upon a decrease of the phenolic content.

In 2011, Song, Guo and co-workers described a phloroglucinol–resin approach, whereby pore diameters of 4.7, 5.5, 12.6 and 17.8 nm were obtained, in this case by adaption of the formaldehyde to surfactant (SDA) ratio.[37] Thereby, the higher the relative loading of the cross-linking formaldehyde component, the smaller the resulting mesopores were found to be. Likely, this is connected to the fact that a high cross-linking density will entail a very compact 3D-connected shell around the self-assembled micellar structures. Interestingly, while the pore size distributions were found to be relatively well-defined, the nitrogen sorption hysteresis loops suggested a difference in pore connectivity between the OMCs derived from high and low formaldehyde loadings.

Also targeting the cross-linking agent, Matei Ghimbeu and co-workers focused on substituting the problematic formaldehyde component by application of glyoxylic acid (Figure 1).[38] Intriguingly, this compound will act both as cross-linker and as a catalyst (via its acid functionality), thus rendering the addition of an external catalyst obsolete. By adaption of the phloroglucinol and glyoxylic acid ratio (1:1.5, 1:1.25, 1:1, molar), pore diameters of 2.7, 2.9 and 6.5 nm could be realized (600 °C). By further adaption of the surfactant loading (reduction of the amount of applied F127), the addressable d_{Meso} could be extended to 8.3 nm. However, the samples did not show the same type of mesostructures. While the latter sample did not display an ordered pore arrangement, as evident by small angle X-ray scattering (SAXS) analysis, the OMC derived from the 1:1 ratio was found to have a 2D hexagonal mesostructure, while the other two samples were of the $Im\bar{3}m$-symmetry, again underlining one of the limitations if pore diameters are to be impacted this way.

Of course, since the polar carbon precursor molecules and the hydrophilic moieties of the SDAs interact in what after carbonization will become the pore wall domains, variation of the corresponding stoichiometry is an excellent approach to also tailor the wall thickness if a suitable polymeric SDA is employed, as demonstrated by Zhao and co-workers in 2009.[39] In this contribution, a poly(ethylene oxide)-*block*-poly(methyl methacrylate)-*block*-poly(styrene) triblock copolymer (PEO_{125}-*b*-$PMMA_{100}$-*b*-PS_{138}) is employed, together with a resol carbon precursor. Using three different heat treatments (450, 800, and 1200 °C), several resol/SDA ratios were investigated with a focus on the resulting pore parameters (0.6–1.4, weight ratio). SAXS patterns revealed a face-centered cubic arrangement which was stable over the whole temperature and composition range; only at the very highest resol loading, this feature starts to get lost. Intriguingly, pore diameters are not correlated with the resol/SDA ratio and also the carbonization temperature displays only a moderate effect: at 450 °C all samples have mean pore sizes of 23.0–23.7 nm, which change to 19.4–20 and 19 nm for the 800 and 1200 °C experiment series, respectively. This is explicitly not the same if wall thicknesses are considered. Here, a range of 11–21 nm is covered, whereby a stepwise increase of resol proportion is mirrored by a stepwise growth of wall thickness. Overall, this interesting behavior was attributed to the characteristics of the applied triblock copolymer. The observed large mesopores are a typical consequence of high-molar mass SDAs (see Section 5). Moreover, this polymer is constructed so that a gradual change of polarity occurs. The middle PMMA block is also of intermediate polarity. Crucially, it was proposed that the resol will preferentially interact with the PEO moieties, but at a high loading it will also start to engage with the PMMA block, thus increasing the hydrophilic volume (which after carbonization will form the carbon framework).

Thus, firstly, it can be summarized that adaption of stoichiometry – regarding important components of the synthetic setup – constitutes a relatively simple, but still limited approach to impact pore sizes. This is in part down to the fact that predominantly the hydrophilic volume is targeted by these variations (and not the lipophilic micellar cores), thus providing only an indirect venue to impact the resulting pore sizes. Secondly, manipulation of pore diameters *within the same mesostructure* is inherently restricted to a suitable window of hydrophilic to lipophilic volume ratios. Thus, as is also evident from some of the examples discussed above, pore size manipulation may be frequently accompanied by a change of the type of pore arrangement (i.e., 2D hexagonal vs. cubic symmetry).

4. Swelling Agents

As a more direct strategy to impact pore diameters, manipulation of the size of micelles, specifically their lipophilic cores, by addition of swelling agents (pore expanders) is both effective and popular. In most cases, no synthetic effort is necessary since commercially available, micelle-forming polymers (i.e., *Pluronics*) can be combined with well available, non-polar swelling agents, whereby the latter can be low-molar-mass organic compounds or oligomeric, short-chain polymers.

Indeed, this strategy is not limited to OMCs, but has earlier been applied to tailor mesoporous silica materials.[40] There, it was found that the uptake of swelling agents into micelles should be finely balanced – the surfactant/SDA must be matched to the swelling agent in a way that defined amounts migrate into the micellar core, while uncontrolled swelling is avoided. Since different surfactants will have different preferences regarding suitable swelling agents, this offers the opportunity to systematically impact micellar sizes. For example, focusing on regular *Pluronics*, it was found that solubilization of simple alkanes and substituted benzenes in PEO-*b*-PPO-*b*-PEO can be rationally tuned (Figure 4). Thus, it makes a difference whether P123 (PEO_{20}-PPO_{70}-PEO_{20}) or F127 (PEO_{106}-PPO_{70}-PEO_{106}) is considered. While the former has about 70 wt% of hydrophobic components (PPO), the latter only displays 30 wt%.[40] Accordingly, swelling agents with lower propensity to solubilize in PEO-*b*-PPO-*b*-PEO are recommended for P123 (cyclohexane, 1,3,5-triisopropylbenzene), while F127 is in need of pore expanders from the more solubilizing end of the scale (such as xylene or toluene).[41,42]

Also for carbon materials systematic investigations have been conducted. Focusing on an OMC–silica hybrid material, Vogt and co-workers used a setup including resol, F127 and tetraethyl orthosilicate plus a number of small-molecule additives to illuminate their performance as swelling agents.[43] Low-volatility additives with different polarity profiles were investigated, using the octanol–water partition coefficient (K_{ow}) as a guideline for hydrophobicity. Thus, applying 1,3,5-trimethylbenzene (TMB; $K_{ow} = 3.42$), d_{Meso} could be increased from 5.9 to 8.1 nm. Application of dioctyl phthalate (DOP; $K_{ow} = 8.1$) even allowed access to mesopores up to 13.5 nm. An even more hydrophobic additive, tris(2-ethyl)trimellitate ($K_{ow} = 12.5$), proved, however, to be less effective, entailing an expansion only up to 8.2 nm. This observation fits well to the above considerations, in that swelling agent and polymer polarity (specifically of the lipophilic moiety) have to be matched to each other. Indeed, when also taking the Hansen solubility parameter into account, a parameter which is usually employed to judge the quality of solvent for a given polymer, it is found that DOP is the best fit to PPO among the swelling agents tested, providing a possible explanation for its excellent ability to tune the pore sizes. It should be noted that significant loadings of DOP can be applied: on going from 0 to 50 wt% (relative to F127), a stepwise increase of d_{Meso} (2D hexagonal arrangement) is observed. At higher loadings, no further pore size growth occurs but the pore size distribution significantly broadens. It should be noted that the presence of swelling agents can not only impact pore sizes, but also the formation mechanism of nanostructures, as was shown by Stein and co-worker for TMB.[44]

Several examples for the application of swelling agents to tailor OMC porosity have been disclosed. For example, in 2006, Zhao and co-workers studied a resol/*Pluronic* system, using decane or hexadecane as hydrocarbon pore extenders.[45] The presence of the swelling agents helped in stabilizing a well-ordered $p\bar{6}mm$-phase, whereby the choice of hydrocarbon allowed for a tailoring of mesopore diameter from 4.1 to 6.8 nm (application of decane delivered the larger mesopores).

Yuan and co-workers described a phloroglucinol/formaldehyde setup based on P123 as SDA.[46] In this case, employing decane as a swelling agent, d_{Meso} was increased from 11.5 to 14.7 nm.

Jaroniec and co-worker used TMB as a swelling agent for a system based on the commercial polymer *Vorasurf 504* (PEO_{38}-PBO_{46}-PEO_{38}, BO = 1-butylene oxide, Dow),[47] thus employing a triblock copolyether with a somewhat more lipophilic middle block compared to regular *Pluronics*. While this particular acid-catalyzed synthesis (resorcinol and formaldehyde) delivered relatively broad pore size distributions and no ordered material, it was nonetheless found that the presence of TMB had a significant impact. Pore sizes increased from 20 to 27 nm (carbonized at 600 °C) and 17 to 23 nm (850 °C), respectively.

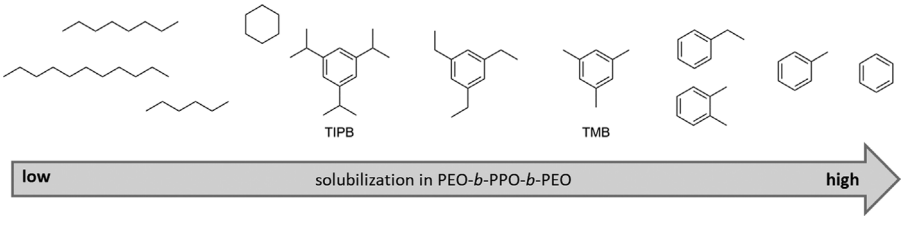

Figure 4 Propensity of different non-polar swelling agents for micellar uptake in *Pluronics*, according to Kruk.[40]

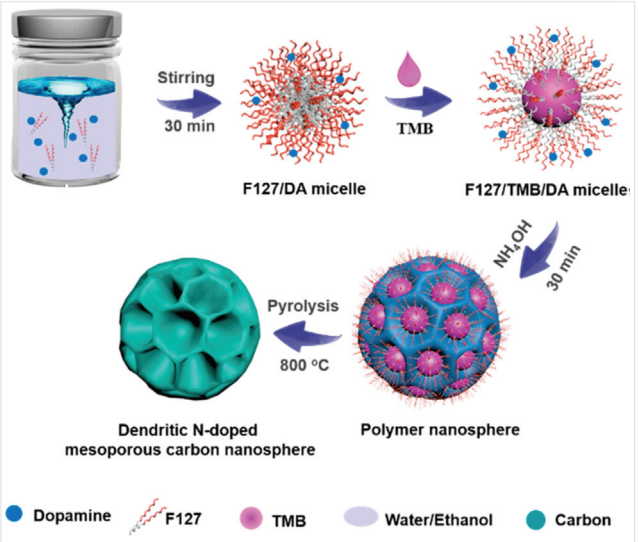

Scheme 2 Nanoemulsion approach for the preparation of *N*-doped mesoporous carbon spheres as described by Li and Zhao. Reprinted with permission from ref. 49. Copyright 2019 American Chemical Society.

Lei and co-workers described an aqueous synthetic route using resorcinol and urotropin (as a source for formaldehyde under acidic conditions) to deliver well-defined OMCs.[48] The addition of TMB was used to entail a different mesophase (2D hexagonal instead of $Im\bar{3}m$-symmetry) with a corresponding increase of pore sizes.

Intriguing *N*-doped mesoporous carbon nanospheres with well-defined and tunable pore sizes were disclosed by Li and Zhao in 2019.[49] In an ethanol/water system, F127 and dopamine were assembled and converted into the corresponding carbon material, supported by the presence of TMB (Scheme 2). The latter not only acted as a swelling agent, but also regulated the SDA/carbon precursor interaction. Hence, the nanospheres resulting from this approach could be directed to display different and novel structures such as smooth, golf ball-like, multichambered or dendritic surface properties. Alongside these changes, also the pore sizes increased [with 5, 13, 21 and 35 nm being reported, depending on the amount of TMB added to the synthetic setup (0.5–2.0 mL)].

An ideal fit of swelling-agent hydrophobicity and the preferences of the micelle-forming amphiphilic polymer is of course given if the pore expander is identical to the lipophilic block of the SDA. Thus, using a PEO-*b*-PS copolymer surfactant, short-chain polystyrene homopolymer (h-PS) seems a promising tool for impacting mesopore diameters.

In 2008, PEO_{125}-*b*-PS_{230} as SDA and resol/THF were applied to generate OMCs, whereby h-PS_{49} was used as a pore expander.[50] Under the preparative conditions reported in this work, it is found that up to 20 wt% of h-PS (relative to the SDA) can be added to still retain a well-ordered face-centered cubic pore arrangement. If the h-PS content is increased stepwise, the mesopore diameter likewise successively increases. Thus, after carbonization at 800 °C, for h-PS loadings of 0, 2, 5, 10 and 20 wt%, d_{Meso} values of 22.9, 28.0, 33.1, 36.9 and 37.4 nm are found, respectively. This impressive list can however not be extended further in this manner, since a higher content of polystyrene pore expander results in less defined, multimodal pores size distributions, broadly in the range of 40–90 nm. It should be noted that the wall thickness is heavily reduced by increasing the ratio of h-PS relative to the other components (only 3.6 nm at 20 wt% loading), hence presenting the possibility to create relatively fragile structures, in contrast to what is usually found for OMCs derived from soft-templating procedures.

Interestingly, Epps, Vogt and co-workers sought to apply the same system for the preparation of OMC thin films.[51] What they found highlights again the considerable differences that can occur between the synthesis of OMC powders and the even more challenging production of well-ordered films. Thus, the authors describe that the pore properties are not impacted by the presence of h-PS up to a loading of 10 wt% and less. In this range of composition the pore size distribution also remains well-controlled. If more h-PS is added, the pore size increases somewhat, but at the same time the pore size distribution also broadens notably. Moreover, the presence of more polystyrene oligomer seems to favor elliptical deformation of the pores. The more pronounced uniaxial shrinkage was attributed to wetting phenomena, which were also thought to be responsible for the absence of any impact on pore sizes at low h-PS loadings.

5. Design of the Polymeric SDAs/Templates

An inherent disadvantage of using swelling agents is that they are not covalently bound to the polymeric SDA. Accordingly, wetting phenomena as described above and phase separations in general can pose a significant difficulty. Furthermore, volatility must be low, because otherwise the additive may evaporate over time or gradually change concentration during the early stages of the preparation process. This may be especially acute if the actual structure formation occurs under thermally induced conditions.[26]

As a viable alternative, the polymer itself can be modified. If controlled polymerization is achieved, the overall molar mass (number-average molar mass, M_n), the relative and absolute size of the lipophilic and hydrophilic blocks as well as the block architecture [diblock (AB), triblock (ABA), reverse triblock (BAB)] can be tailored. Also, more than two types of monomer can be employed, allowing access, for example, to ABC triblock copolymers with a gradual change in polarity. In general terms, this

means that crucial parameters such as mesostructure, wall thickness and mesopore diameter should be readily controllable.

It should also be noted that the additional synthetic effort – often perceived as an important drawback in comparison to the application of commercial polymer SDAs – is usually well manageable, helped by the advent of more user-friendly and precise polymerization techniques and catalysts.

An instructive case in point is found in *Pluronics*. While being cheap and available in a number of grades,[52] the commercial product is also subject to a number of limitations, including for example low molar masses (<13 kg/mol maximum) and small block lengths of the lipophilic PPO moieties ($n \leq 70$). Both points are decisive for mesopore generation: the lipophilic volume for directly impacting d_{Meso}, and the PEO for managing suitable ratios (HLB) to address the desired mesostructure, among other factors.

One of the consequences is that *Pluronic*-templated OMCs have usually relatively small mesopores (<8 nm) and might require the addition of swelling agents if larger dimensions are desired. It is therefore no coincidence that F127 and P123 ($n = 70$) are amongst the most popular polymers of this SDA family for soft-templating OMCs.

Recent progress in the preparation of polyethers, however, has rendered much higher molar masses and significantly enlarged PPO blocks accessible,[53–55] for example in the form of so-called *Reverse Pluronics* (PPO-*b*-PEO-*b*-PPO, Scheme 3a). Extensive libraries of these polyethers have been created[56] and successful examples for their employment as SDAs to generate OMCs via soft-templating exist.[57–59] Notably, it is possible to apply very simple and robust catalyst systems to prepare PPO_n-*b*-PEO_m-*b*-PPO_n with excellent molar mass distribution ($Đ_M \leq 1.03$, n up to 135), using well-available nitrogen bases such as 1,8-diazabicyclo[5.4.0]undec-7-ene (DBU), 4-dimethylaminopyridine (DMAP) or 1,4-diazabicyclo [2.2.2]octane (DABCO).[60]

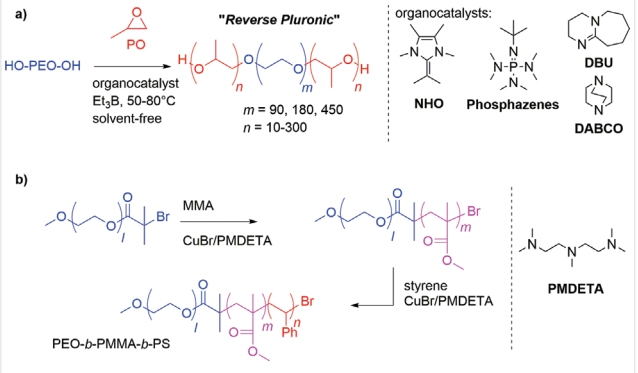

Scheme 3 Access to high molar-mass *Reverse Pluronics* via organopolymerization (a)[60] and ATRP-based ABC-triblock copolymer (b).[39] NHO = *N*-heterocyclic olefin.

Further, living radical polymerization [i.e., atom transfer radical polymerization (ATRP) or reversible-addition–fragmentation chain-transfer polymerization] has been employed to prepare polymer SDAs, such as poly(acrylonitrile)-based setups.[61–63] Another example already mentioned above is PEO_{125}-*b*-$PMMA_{100}$-*b*-PS_{138}, whereby sequential polymerization of MMA and styrene (starting from PEO-Br as macroinitiator, Scheme 3b) was conducted.[39] Likewise, PEO-*b*-PS is readily accessible via ATRP.[51] Hence, in view of operationally simple procedures such as these and others, the tailoring of the structure-directing amphiphilic polymers has developed to be the most promising and most immediate approach to actually design OMC porosity; in the ideal case, a high degree of control over the polymerization process is directly translated into control over mesopore development.

For example, in 2010, resol/PEO_{125}-*b*-PS_n with different degrees of polymerization of the hydrophobic PS moiety ($n = 120, 250, 305$) was employed to generate OMC with $Im\bar{3}m$-type symmetry.[64] Crucially, d_{Meso} was readily manipulated via the rigid PS-moieties: dimensions of 11.9, 22.7 and 33.3 nm were found for the three different PS block lengths, respectively. The larger mesopores accordingly enforced gradually thinning pore-wall thicknesses (11.3 10.0, 5.3 nm). The material was subsequently oxidized (using HNO_3/H_2O_2 mixtures) without destroying the large-pore mesostructure and then loaded with nanoparticles (Ag, Fe).

Mai and co-workers applied the same type of polymer SDA for the preparation of nitrogen-doped mesoporous carbon nanospheres with controllable pore diameters (Table 2).[65] This setup was based on the co-assembly of (poly)dopamine and PEO_{114}-*b*-PS_n. Interestingly, the authors found a linear dependence of d_{Meso} on the square root of n ($R^2 = 0.98$).

Extending this system to a triblock copolymer, Wiesner and co-workers applied poly(isoprene)-*block*-poly(styrene)-*block*-poly(ethylene oxide) (PI-*b*-PS-*b*-PEO) for the preparation of gyroidal OMCs with large mesopore diameters.[66] Note that in this case, sequential anionic polymerization was employed to prepare excellently defined SDAs ($Đ_M = 1.04–1.07$), hence in the sequence of synthesis the PEO block is generated last.[67] It was demonstrated that, by keeping constant the volume

Table 2 *N*-Doped carbon nanospheres derived from PEO-*b*-PS as reported by Mai[65]

SDA	d_{Meso} [nm][a]	SSA [m^2/g][b]	V_{total} [cm^3/g]
PEO_{114}-*b*-PS_{60}	8	450	0.50
PEO_{114}-*b*-PS_{153}	15	362	0.71
PEO_{114}-*b*-PS_{255}	23	342	0.96
PEO_{114}-*b*-PS_{341}	28	276	0.64
PEO_{114}-*b*-PS_{390}	33	229	0.60

[a]Determined via nitrogen sorption.
[b]SSA = specific surface area.

fractions of the components [f(PI) = 17%, f(PS) = 32%, f(PEO) = 51%], but increasing the overall molar mass in steps (M_n = 39,56,108 kg/mol), the mesopore size could be tailored nicely; indeed, after carbonization at 900 °C, a d_{Meso} of 15, 19 and 39 nm was observed, respectively. Even at 1600 °C, relatively well-defined porosity was found, albeit with broader pore size distribution and decreased long-range order.

In 2011, Zhao and co-workers studied PEO-*b*-PMMA as a polymer SDA (prepared via ATRP).[68] It was observed that the pore size increased from 8.6 to 12.1 nm (450 °C) as the PMMA block length was extended (PEO_{44}-*b*-$PMMA_{103}$ vs. PEO_{125}-*b*-$PMMA_{174}$), representing an early example for hexagonal $p\bar{6}mm$-symmetry with relatively large, cylindrical mesopores. By the addition of PMMA homopolymer (9 kg/mol) as a pore expander, a mesopore-diameter range of overall 8.6–22.0 nm could be covered.

Using a more unusual approach, Watkins and co-workers employed bottlebrush block copolymers to access a wide range of pore diameters, exceeding the mesopore domain (18–150 nm).[69] Thus, under sequential application of norbornene-capped poly(dimethylsiloxane) (PDMS; 4.8 kg/mol) and norbornene-capped PEO (5.0 kg/mol), ring-opening metathesis polymerization (Grubbs-type catalysts) delivered the desired block copolymers, whereby a series of compounds with constant mass fractions (50:50, PDMS:PEO) but increasing molar masses was prepared. Thus, the corresponding PDMS-*b*-PEO bottlebrush copolymers with very high M_n = 210, 250, 394, 640 and 1800 kg/mol were applied for structure direction in combination with resol as a carbon precursor. Notably, in stark contrast to rigid PS-blocks, the non-polar PDMS is highly flexible. This was thought to facilitate the formation of mesostructures with a high curvature. Furthermore, upon heating above 420 °C, PDMS degrades over several steps into volatile, cyclic compounds. This process is relatively slow (but almost quantitative), which is beneficial for the conservation of ordered structures. The self-assembly delivers well-ordered, spherical morphologies (Figure 5), and crucially the diameter of the PDMS spheres is linearly dependent on the molar mass of the bottlebrush SDA. This can be directly translated into likewise control over the mesopores, allowing access to pore sizes of 15.7, 22.1, 32.7, 49.0 and 107.7 nm for the different grades of PDMS-*b*-PEO, respectively.

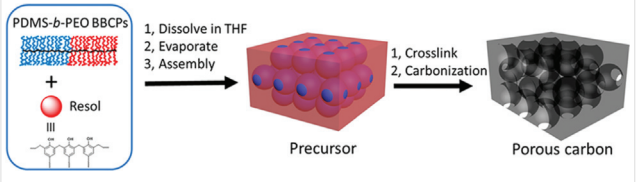

Figure 5 Nanoporous, well-ordered carbon material as derived by application of tailored PDMS-*b*-PEO bottlebrush SDAs, according to Watkins. Adapted with permission from ref. 69. Copyright 2019 American Chemical Society.

Progress in related fields of research may provide an outlook on what may be possible in the near future by pushing polymer SDA design to even more sophisticated levels. Thus, in a recently published work by Andrieu-Brunsen and Gallei, it is demonstrated how polymers consisting for example of lipophilic PS and hydrophilic poly(2-vinylpyridine) blocks, end-functionalized with triethoxysilane, allow for the preparation of well-defined films of mesoporous silica.[70] Importantly, the polymer not only acts as SDA, but is also directly incorporated into the pore wall. Positioned in such a way, the polymers can be used to infringe d_{Meso}, but also to impact transport properties of, for example, ionic species when the pH is modulated (protonation of the pyridine motifs). Similar in-situ approaches for the preparation of OMCs would be tremendously useful, not least because this way functional groups could be homogeneously distributed along the pore wall, avoiding clustering at the pore mouth (as may be the case for post-functionalization strategies).

6. Conclusions and Outlook

Without doubt, OMCs will continue on their successful journey, not least since it can be safely assumed that their potential is far from being fully realized yet. Such progress will go alongside the development of ever more precise synthetic procedures, including also better control over the mesopore dimensions. Inventive ways to functionalize/dope the material surface will also contribute to this development.[71,72] While the generation of mesostructured carbons via soft-templating is a delicate process, and thereby susceptible to many venues of property manipulation, the most direct route to control features such as mesopore diameter is surely given by impacting the self-assembly of micellar systems. It is therefore no coincidence that such strategies, as embodied by approaches using swelling agents or tailored polymers as templates, have found particular interest. They are especially useful for screening OMCs with gradually different mesopore sizes while staying within the same type of mesostructure/pore arrangement with the same type and density of surface functional groups. Such a systematic variation of otherwise truly uniform materials is of supreme importance if size-dependent effects are to be identified and quantified; such phenomena include confinement effects in catalysis[73] or energy density in electrode materials,[74] but can in principle be envisioned for a wide range of high-tech applications. Thus, novel and yet unexpected developments in (meso)pore size control can be expected in the near future and will be highly relevant, both for academia and industry.

Funding Information

This study was funded by the Deutsche Forschungsgemeinschaft (DFG, German Research Foundation) – Project-ID 358283783–SFB 1333.

Acknowledgment

The University of Stuttgart is gratefully acknowledged for Open Access funding.

References

(1) Zhao, D.; Zhou, W.; Wan, Y. Ordered Mesoporous Materials. Wiley-VCH Verlag GmbH & Co. KGaA: Weinheim, **2013**; Chap. 8,: 293–341.
(2) Stein, A.; Wang, Z.; Fierke, M. A. *Adv. Mater.* **2009**, *21*, 265.
(3) Liang, C.; Li, Z.; Dai, S. *Angew. Chem. Int. Ed.* **2008**, *47*, 3696.
(4) Xin, W.; Song, Y. *RSC Adv.* **2015**, *5*, 83239.
(5) Panja, T.; Bhattacharjya, D.; Yu, J.-S. *J. Mater. Chem. A* **2015**, *3*, 18001.
(6) Feng, D.; Lv, Y.; Wu, Z.; Dou, Y.; Han, L.; Sun, Z.; Xia, Y.; Zheng, G.; Zhao, D. *J. Am. Chem. Soc.* **2011**, *133*, 15148.
(7) Hao, G.-P.; Li, W.-C.; Qian, D.; Wang, G.-H.; Zhang, W.-P.; Zhang, T.; Wang, A.-Q.; Schüth, F.; Bongard, H.-J.; Lu, A.-H. *J. Am. Chem. Soc.* **2011**, *133*, 11378.
(8) Fang, Y.; Gu, D.; Zou, Y.; Wu, Z.; Li, F.; Che, R.; Deng, Y.; Tu, B.; Zhao, D. *Angew. Chem. Int. Ed.* **2010**, *49*, 7987.
(9) Benzigar, M. R.; Talapaneni, S. N.; Joseph, S.; Ramadass, K.; Singh, G.; Scaranto, J.; Ravon, U.; Al-Bahily, K.; Vinu, A. *Chem. Soc. Rev.* **2018**, *47*, 2680.
(10) Borchardt, L.; Oschatz, M.; Kaskel, S. *Chem. Eur. J.* **2016**, *22*, 7324.
(11) Zhang, L. L.; Zhao, X. S. *Chem. Soc. Rev.* **2009**, *38*, 2520.
(12) Chang, H.; Joo, S. H.; Pak, C. *J. Mater. Chem.* **2007**, *17*, 3078.
(13) Daems, N.; Sheng, X.; Vankelecom, I. F. J.; Pescarmona, P. P. *J. Mater. Chem. A* **2014**, *2*, 4085.
(14) Perreault, L. L.; Giret, S.; Gagnon, M.; Florek, J.; Larivière, D.; Kleitz, F. *ACS Appl. Mater. Interfaces* **2017**, *9*, 12003.
(15) Zheng, B.; Lin, X.; Zhang, X.; Wu, D.; Matyjaszewski, K. *Adv. Funct. Mater.* **2020**, *30*, 1907006.
(16) Liang, C.; Hong, K.; Guiochon, G. A.; Mays, J. W.; Dai, S. *Angew. Chem. Int. Ed.* **2004**, *43*, 5785.
(17) Tanaka, S.; Nishiyama, N.; Egashira, Y.; Ueyama, K. *Chem. Commun.* **2005**, 2125.
(18) Wan, Y.; Shi, Y.; Zhao, D. *Chem. Mater.* **2008**, *20*, 932.
(19) Brinker, C. J.; Lu, Y.; Sellinger, A.; Fan, H. *Adv. Mater.* **1999**, *11*, 579.
(20) Xia, Y.; Yang, Z.; Mokaya, R. *Nanoscale* **2010**, *2*, 639.
(21) Ma, T.-Y.; Liu, L.; Yuan, Z.-Y. *Chem. Soc. Rev.* **2013**, *42*, 3977.
(22) Chuenchom, L.; Kraehnert, R.; Smarsly, B. M. *Soft Matter* **2012**, *8*, 10801.
(23) Petkovich, N. D.; Stein, A. *Chem. Soc. Rev.* **2013**, *42*, 3721.
(24) Liang, C.; Dai, S. *J. Am. Chem. Soc.* **2006**, *128*, 5316.
(25) Zhang, F.; Meng, Y.; Gu, D.; Yan, Y.; Yu, C.; Tu, B.; Zhao, D. *J. Am. Chem. Soc.* **2005**, *127*, 13508.
(26) Schuster, J.; Köhn, R.; Döblinger, M.; Keilbach, A.; Amenitsch, H.; Bein, T. *J. Am. Chem. Soc.* **2012**, *134*, 11136.
(27) Doncom, K. E. B.; Blackman, L. D.; Wright, D. B.; Gibson, M. I.; O'Reilly, R. K. *Chem. Soc. Rev.* **2017**, *46*, 4119.
(28) Kondrat, S.; Pérez, C. R.; Presser, V.; Gogotsi, Y.; Kornyshev, A. A. *Energy Environ. Sci.* **2012**, *5*, 6474.
(29) Merlet, C.; Péan, C.; Rotenberg, B.; Madden, P. A.; Daffos, B.; Taberna, P.-L.; Simon, P.; Salanne, M. *Nat. Commun.* **2013**, *4*, 2701.
(30) Wang, X.; Liang, C.; Dai, S. *Langmuir* **2008**, *24*, 7500.
(31) Liu, C.; Li, L.; Song, H.; Chen, X. *Chem. Commun.* **2007**, 757.
(32) Meng, Y.; Gu, D.; Zhang, F.; Shi, Y.; Yang, H.; Li, Z.; Yu, C.; Tu, B.; Zhao, D. *Angew. Chem. Int. Ed.* **2005**, *44*, 7053.
(33) Meng, Y.; Gu, D.; Zhang, F.; Shi, Y.; Cheng, L.; Feng, D.; Wu, Z.; Chen, Z.; Wan, Y.; Stein, A.; Zhao, D. Y. *Chem. Mater.* **2006**, *18*, 4447.
(34) Libbrecht, W.; Verberckmoes, A.; Thybaut, J. W.; Van Der Voort, P.; De Clercq, J. *Langmuir* **2017**, *33*, 6769.
(35) Jin, J.; Nishiyama, N.; Egashira, Y.; Ueyama, K. *Microporous Mesoporous Mater.* **2009**, *118*, 218.
(36) Mitome, T.; Hirota, Y.; Uchida, Y.; Nishiyama, N. *Colloids Surf., A* **2016**, *494*, 180.
(37) Li, P.; Song, Y.; Guo, Q.; Shi, J.; Liu, L. *Mater. Lett.* **2011**, *65*, 2130.
(38) Matei Ghimbeu, C.; Vidal, L.; Delmotte, L.; Le Meins, J.-M.; Vix-Guterl, C. *Green Chem.* **2014**, *16*, 3079.
(39) Zhang, J.; Deng, Y.; Wei, J.; Sun, Z.; Gu, D.; Bongard, H.; Liu, C.; Wu, H.; Tu, B.; Schüth, F.; Zhao, D. *Chem. Mater.* **2009**, *21*, 3996.
(40) Kruk, M. *Acc. Chem. Res.* **2012**, *45*, 1678.
(41) Cao, L.; Man, T.; Kruk, M. *Chem. Mater.* **2009**, *21*, 1144.
(42) Huang, L.; Yan, X.; Kruk, M. *Langmuir* **2010**, *26*, 14871.
(43) Trivedi, M.; Peng, F.; Xia, X.; Sepulveda-Medina, P. I.; Vogt, B. D. *Langmuir* **2019**, *35*, 14049.
(44) Wang, Z.; Stein, A. *Chem. Mater.* **2008**, *20*, 1029.
(45) Zhang, F.; Meng, Y.; Gu, D.; Yan, Y.; Chen, Z.; Tu, B.; Zhao, D. *Chem. Mater.* **2006**, *18*, 5279.
(46) Liu, L.; Wang, F.-Y.; Shao, G.-S.; Ma, T.-Y.; Yuan, Z.-Y. *Carbon* **2010**, *48*, 2660.
(47) Wickramaratne, N. P.; Jaroniec, M. *Carbon* **2013**, *51*, 45.
(48) Liu, D.; Lei, J.-H.; Guo, L.-P.; Qu, D.; Li, Y.; Su, B.-L. *Carbon* **2012**, *50*, 476.
(49) Peng, L.; Hung, C.-T.; Wang, S.; Zhang, X.; Zhu, X.; Zhao, Z.; Wang, C.; Tang, Y.; Li, W.; Zhao, D. *J. Am. Chem. Soc.* **2019**, *141*, 7073.
(50) Deng, Y.; Liu, J.; Liu, C.; Gu, D.; Sun, Z.; Wei, J.; Zhang, J.; Zhang, L.; Tu, B.; Zhao, D. *Chem. Mater.* **2008**, *20*, 7281.
(51) Labiano, A.; Dai, M.; Young, W.-S.; Stein, G. E.; Cavicchi, K. A.; Epps, T. H.; Vogt, B. D. *J. Phys. Chem. C* **2012**, *116*, 6038.
(52) Herzberger, J.; Niederer, K.; Pohlit, H.; Seiwert, J.; Worm, M.; Wurm, F. R.; Frey, H. *Chem. Rev.* **2016**, *116*, 2170.
(53) Naumann, S.; Thomas, A. W.; Dove, A. P. *Angew. Chem. Int. Ed.* **2015**, *54*, 9550.
(54) Zhang, C.-J.; Duan, H.-Y.; Hu, L.-F.; Zhang, C.-H.; Zhang, X.-H. *ChemSusChem* **2018**, *11*, 4209.
(55) Chen, Y.; Shen, J.; Liu, S.; Zhao, J.; Wang, Y.; Zhang, G. *Macromolecules* **2018**, *51*, 8286.
(56) Markus, F.; Bruckner, J. R.; Naumann, S. *Macromol. Chem. Phys.* **2020**, *221*, 1900437.
(57) Huang, Y.; Cai, H.; Yu, T.; Zhang, F.; Zhang, F.; Meng, Y.; Gu, D.; Wan, Y.; Sun, X.; Tu, B.; Zhao, D. *Angew. Chem. Int. Ed.* **2007**, *46*, 1089.
(58) Li, P.; Song, Y.; Lin, Q.; Shi, J.; Liu, L.; He, L.; Ye, H.; Guo, Q. *Microporous Mesoporous Mater.* **2012**, *159*, 81.
(59) Balint, A.; Papendick, M.; Clauss, M.; Müller, C.; Giesselmann, F.; Naumann, S. *Chem. Commun.* **2018**, *54*, 2220.
(60) Vogler, C.; Naumann, S. *RSC Adv.* **2020**, *10*, 43389.
(61) Kowalewski, T.; Tsarevsky, N. V.; Matyjaszewski, K. *J. Am. Chem. Soc.* **2002**, *124*, 10632.

(62) Zhou, Z.; Liu, G. *Small* **2017**, *13*, 1603107.
(63) Kopeć, M.; Lamson, M.; Yuan, R.; Tang, C.; Kruk, M.; Zhong, M.; Matyjaszewski, K.; Kowalewski, T. *Prog. Polym. Sci.* **2019**, *92*, 89.
(64) Deng, Y.; Cai, Y.; Sun, Z.; Gu, D.; Wei, J.; Li, W.; Guo, X.; Yang, J.; Zhao, D. *Adv. Funct. Mater.* **2010**, *20*, 3658.
(65) Tian, H.; Lin, Z.; Xu, F.; Zheng, J.; Zhuang, X.; Mai, Y.; Feng, X. *Small* **2016**, *12*, 3155.
(66) Werner, J. G.; Hoheisel, T. N.; Wiesner, U. *ACS Nano* **2014**, *8*, 731.
(67) Bailey, T. S.; Hardy, C. M.; Epps, T. H.; Bates, F. S. *Macromolecules* **2002**, *35*, 7007.
(68) Wei, J.; Deng, Y.; Zhang, J.; Sun, Z.; Tu, B.; Zhao, D. *Solid State Sci.* **2011**, *13*, 784.
(69) Fei, H.-F.; Li, W.; Bhardwaj, A.; Nuguri, S.; Ribbe, A.; Watkins, J. J. *J. Am. Chem. Soc.* **2019**, *141*, 17006.
(70) Herzog, N.; Hübner, H.; Rüttiger, C.; Gallei, M.; Andrieu-Brunsen, A. *Langmuir* **2020**, *36*, 4015.
(71) Dou, S.; Tao, L.; Wang, R.; El Hankari, S.; Chen, R.; Wang, S. *Adv. Mater.* **2018**, *30*, 1705850.
(72) Yu, F.; Liu, M.; Ma, C.; Di, L.; Dai, B.; Zhang, L. *Nanomaterials* **2019**, *9*, 1436.
(73) Ziegler, F.; Teske, J.; Elser, I.; Dyballa, M.; Frey, W.; Kraus, H.; Hansen, N.; Rybka, J.; Tallarek, U.; Buchmeiser, M. R. *J. Am. Chem. Soc.* **2019**, *141*, 19014.
(74) Kondrat, S.; Pérez, C. R.; Presser, V.; Gogotsi, Y.; Kornyshev, A. A. *Energy Environ. Sci.* **2012**, *5*, 6474.